



ELSEVIER

Contents lists available at ScienceDirect

Materials Letters

journal homepage: www.elsevier.com/locate/matlet

Fabrication and photoelectrochemical studies of $\text{Bi}_2\text{Ti}_2\text{O}_7$ pyrochlore thin films by aerosol assisted chemical vapour deposition

Andrew McInnes, Jagdeep S. Sagu, K.G.U. Wijayantha*

Energy Research Laboratory, Department of Chemistry, Loughborough University, Loughborough LE11 3TU, United Kingdom

ARTICLE INFO

Article history:

Received 11 July 2014

Accepted 28 August 2014

Available online 6 September 2014

Keywords:

Photoelectrochemical

Semiconductor

Thin film

ABSTRACT

Phase pure thin film $\text{Bi}_2\text{Ti}_2\text{O}_7$ photoelectrodes were produced by aerosol assisted chemical vapour deposition at 600 °C for the first time. X-ray diffraction analysis showed that the as-deposited $\text{Bi}_2\text{Ti}_2\text{O}_7$ films were amorphous in nature; however, post-deposition annealing at 600 °C for 12 h significantly increased the crystallinity to give phase pure $\text{Bi}_2\text{Ti}_2\text{O}_7$. Scanning electron microscopy revealed that the as-deposited film had a cauliflower-like structure with features ranging from 0.5 to 1.0 μm in size. It was found that the post-annealing step sintered the features together reducing the pores in the structure and giving rise to larger features of 1.0–2.0 μm in size. Optical studies showed that the $\text{Bi}_2\text{Ti}_2\text{O}_7$ film had a direct band gap of 2.74 eV. The photoelectrochemical properties of $\text{Bi}_2\text{Ti}_2\text{O}_7$ were tested and it was found that the electrodes exhibited a photocurrent density of 1.8 $\mu\text{A cm}^{-2}$ at 0.23 V vs. Ag/AgCl. Results showed that $\text{Bi}_2\text{Ti}_2\text{O}_7$ is an attractive material for photoelectrochemical water splitting.

© 2014 The Authors. Published by Elsevier B.V. This is an open access article under the CC BY license (<http://creativecommons.org/licenses/by/3.0/>).

1. Introduction

Pyrochlores are a class of material with the general structure $\text{A}_2\text{B}_2\text{O}_7$ which consists of an interpenetrating cuprite-type A_2O tetrahedral framework with a corner sharing BO_6 octahedron [1]. Bismuth based pyrochlores, in general, have been attracting interest for many diverse applications such as ceramic capacitors, piezoelectric transducers, sensors and dynamic random access memories, due to their high dielectric constants and ferroelectric properties [2]. The photocatalytic properties of $\text{Bi}_2\text{Ti}_2\text{O}_7$ in particular have been attractive due to the fact that it has a narrower band gap (~ 2.8 eV) than that of widely studied TiO_2 [3,4] whilst maintaining suitable band energetics (i.e. for water splitting reactions). The relatively narrow band gap is achieved by the upward shift in the valence band energy from the Bi 6s orbital [5]. It has also been demonstrated that $\text{Bi}_2\text{Ti}_2\text{O}_7$ has excellent photo and chemical stability and electron–hole pairs generated under illumination have long life-times [6,7] which should partly resolve the problems associated with electron–hole recombination, especially as it has been shown that p-block elements, such as Bi, show high electron mobility compared to TiO_2 [8]. Two recent reports have shown that incorporation of Mn and Fe into the structure can result in further narrowing of the band gap to as small as 2.1 eV [3,4]. Whilst there have been a number of reports on the photocatalytic activity of $\text{Bi}_2\text{Ti}_2\text{O}_7$; to the best of our knowledge, there is

only one previous report for use in water splitting cells using thin film electrodes, which was published during the review process of the present paper [9].

There are a number of reported synthesis methods for $\text{Bi}_2\text{Ti}_2\text{O}_7$ in the literature, such as co-precipitation [10], metal-organic deposition [11], and sol–gel [2]. However the majority of methods reported in the literature are aimed at preparing the material in the form of a powder (at micro- and nano-scale) rather than thin films. A common problem associated with the existing methods for thin film fabrication is achieving a pure phase, as, for example, impurity phases such as $\text{Bi}_4\text{Ti}_3\text{O}_{12}$ have been often observed in the powder synthesis [12]. Aerosol assisted chemical vapour deposition (AACVD) is a relatively simple and highly versatile method for the fabrication of highly nanostructured thin films [13–15]. The method allows deposition of multicomponent films from a single precursor solution and the nanostructure can easily be controlled by carefully selecting the solvent and tuning the concentration, temperature and the deposition flow rates.

In this study, we have prepared phase pure $\text{Bi}_2\text{Ti}_2\text{O}_7$ thin films by the method of AACVD and characterised them by XRD, SEM and diffuse absorbance spectroscopy. We also report the photoelectrochemical properties of $\text{Bi}_2\text{Ti}_2\text{O}_7$ thin films.

2. Experimental

AACVD was used to fabricate thin films of $\text{Bi}_2\text{Ti}_2\text{O}_7$; a detailed description of the experimental setup and theory is given elsewhere

* Corresponding author. Tel.: +44 1509 222574; fax: +44 1509 223925.

E-mail address: U.Wijayantha@lboro.ac.uk (K.G.U. Wijayantha).

[16,17]. Briefly, a flask containing the AACVD precursor (40 cm^3) solution was placed above a piezoelectric transducer to generate an aerosol. Air ($109 \text{ cm}^3 \text{ min}^{-1}$) was used as the carrier gas to transfer the aerosol to a second flask where the larger droplets fall out of the stream. A secondary flow of air ($2340 \text{ cm}^3 \text{ min}^{-1}$) was used to transfer the finer aerosol droplets onto an FTO substrate (TEC 8 Pilkington, $8 \Omega/\text{sq}$), which was heated by a hotplate to 600°C . The aerosol decomposed on the hotplate to give the desired thin film. The AACVD precursor solution was prepared by dissolving bismuth nitrate pentahydrate (0.02 mol) in acetylacetone (7.0 cm^3), after which it was diluted by the addition of methanol (50 cm^3), then titanium isopropoxide ($6.75 \times 10^{-3} \text{ mol}$) was added and the solution was then made up to 100 cm^3 by addition of methanol. The FTO coated glass was cut ($1 \times 2 \text{ cm}^2$) and ultrasonically cleaned with doubly distilled water, acetone, propan-2-ol and ethanol prior to use. All chemicals were purchased from Sigma Aldrich and were of 99% purity or higher. The deposition process was carried out for 1 h to obtain a film with an appropriate thickness (approx. $1 \mu\text{m}$). A post-deposition annealing step, typically 12 h at 600°C , was used to improve the crystallinity of $\text{Bi}_2\text{Ti}_2\text{O}_7$ thin films.

The phase and crystallinity of the films were characterised using a Bruker AXS Advance X-ray diffractometer with primary monochromatic high intensity $\text{Cu K}\alpha$ ($\lambda = 1.541 \text{ \AA}$) radiation. The current–voltage (J – V) characteristics of the $\text{Bi}_2\text{Ti}_2\text{O}_7$ thin films were tested using Galvanostat/Potentiostat (Eco Chemie micro-Autolab type III), under illumination by an AM 1.5 Class A solar simulator (Solar Light 16S – 300 solar simulator), at 100 mW cm^{-2} light intensity, calibrated by a silicon pyranometer (Solar Light Co., PMA2144 Class II). The films were measured in a standard, three-electrode configuration in a quartz cell using a platinum wire counter-electrode and a Ag/AgCl/3M KCl reference electrode. The electrolyte was 1 M sodium hydroxide and the scan rate was maintained at 10 mV s^{-1} . Diffuse absorbance measurements were carried out on a Lambda 35 Perkin-Elmer UV/Vis Spectrometer. The surface morphology was studied using a Leo 1530 VP field emission gun scanning electron microscope (FEG-SEM) at an accelerating voltage of 5 kV and a working distance of 5 mm.

3. Results and discussion

$\text{Bi}_2\text{Ti}_2\text{O}_7$ thin films were produced by AACVD at 600°C on FTO glass substrates. Fig. 1 shows the X-ray diffraction (XRD) patterns of an as-deposited thin film and a film after 12 h of post-deposition annealing at 600°C . The XRD pattern for the as-deposited films show peaks only from the F:SnO_2 layer from the substrate. The peaks at 26.8° , 34.0° , 38.0° , 51.7° , 54.7° , 61.7° and 65.7° correspond to the (110), (101), (111), (211), (220), (310) and (301) reflections of SnO_2 , respectively (ICDD 00-041-1445). This showed that the as-deposited film had an amorphous nature. To increase the crystallinity of the thin film, it was subjected to post-deposition annealing for 12 h at 600°C . The XRD pattern for the post-annealed indicated the presence of a cubic $\text{Bi}_2\text{Ti}_2\text{O}_7$ phase, with peaks at 15.0° , 27.3° , 28.8° , 30.1° , 34.8° , 38.0° , 46.0° , 49.9° , 51.9° , 59.4° and 62.4° corresponding to the (222), (620), (622), (444), (800), (622), (1022), (880), (1062), (1244) and (888) reflections of $\text{Bi}_2\text{Ti}_2\text{O}_7$, respectively (ICDD 00-032-0118). The XRD pattern shows no other reflections for impurities such as TiO_2 , Bi_2O_3 or $\text{Bi}_4\text{Ti}_3\text{O}_{12}$.

The surface morphology of the thin films before and after the post-deposition annealing step was studied by FEG-SEM and are shown in Fig. 2a and b, respectively. It can be seen that the $\text{Bi}_2\text{Ti}_2\text{O}_7$ film consists of cauliflower shaped structures ranging in size from 0.5 to $1 \mu\text{m}$.

A cross-sectional image of a post-annealed film is shown in Fig. 2c, which shows a film thickness of around $1 \mu\text{m}$ after 60 min

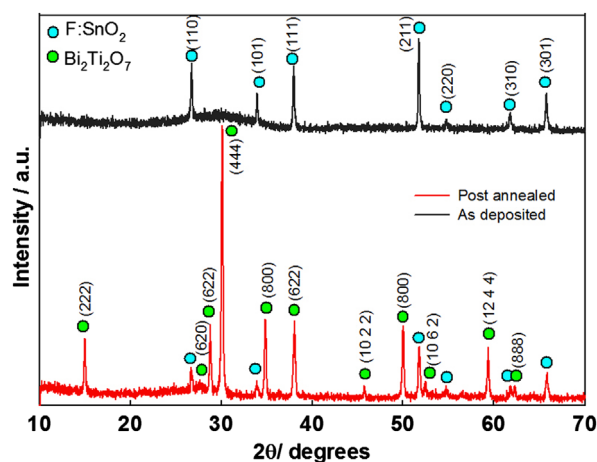


Fig. 1. X-ray diffraction pattern of the as-deposited (black) and post-annealed (red) $\text{Bi}_2\text{Ti}_2\text{O}_7$ thin film. (For interpretation of the reference to colour in this figure legend, the reader is referred to the web version of this article.)

of deposition by AACVD. It can be seen that post-deposition annealing for 12 h at 600°C causes sintering of the nanostructure, resulting in the formation of larger size features in the range of 1 – $2 \mu\text{m}$, compared to the 0.5 – $1 \mu\text{m}$ size before annealing. Also, it can be seen that there is a reduction in void space between the individual features after annealing, which may result in lowering the surface area.

Diffuse absorbance measurements were carried out on post-annealed films. Fig. 3 shows the absorbance spectrum for $\text{Bi}_2\text{Ti}_2\text{O}_7$ and it can be seen that the optical absorption onset occurs at around 430 nm . It has been shown by several previous studies that $\text{Bi}_2\text{Ti}_2\text{O}_7$ is a direct band gap semiconductor and so a plot of $(\alpha h\nu)^{0.5}$ vs. photon energy (Tauc plot) can be used to estimate the band gap of $\text{Bi}_2\text{Ti}_2\text{O}_7$ [1]. In the present work, the band gap was estimated to be 2.74 eV , which also agreed with the recently reported work [3].

The PEC properties of the $\text{Bi}_2\text{Ti}_2\text{O}_7$ were investigated in 1 M NaOH aqueous electrolyte under AM 1.5G illumination. The chopped photocurrent–voltage curve is shown in Fig. 4. The photocurrent onset occurs at around -0.38 V vs. Ag/AgCl , and the films showed a photocurrent of $1.8 \mu\text{A cm}^{-2}$ at 0.23 V vs. Ag/AgCl (1.23 V vs. NHE), which increased to around $3 \mu\text{A cm}^{-2}$ up to the dark current onset at 0.7 V vs. Ag/AgCl [18]. The photocurrent corresponds to water oxidation under illumination. Unlike other well studied materials such as TiO_2 [18] there were no signs of recombination in the $\text{Bi}_2\text{Ti}_2\text{O}_7$ film under the chopped illumination. Usually, in the presence of recombination in an n-type semiconductor, positive spikes in the photocurrent transients are observed under illumination (termed the instantaneous hole current), which decays to a steady state current after recombination with electrons then, when the illumination is interrupted, the hole current ceases immediately and the trapped holes recombine with electrons giving a current spike in the negative direction [19,20]. The absence of these recombination features illustrates that the electron–hole lifetime is indeed longer in $\text{Bi}_2\text{Ti}_2\text{O}_7$ than in TiO_2 and suggests that the electron mobility may be higher in Bi based pyrochlores compared to TiO_2 as already reported in the literature [6,7].

Also, it is known that direct band gap materials are likely to be more efficient in photocatalytic and PEC applications compared with indirect band gap materials as it minimises recombination due to trapping of excited electrons as they move from the valence band to the conduction band [1]. This makes $\text{Bi}_2\text{Ti}_2\text{O}_7$ a good material for such applications. The photocurrent onset method can be used to estimate the flatband potential of $\text{Bi}_2\text{Ti}_2\text{O}_7$, so as can be seen from the inset of Fig. 4, the flatband potential can be

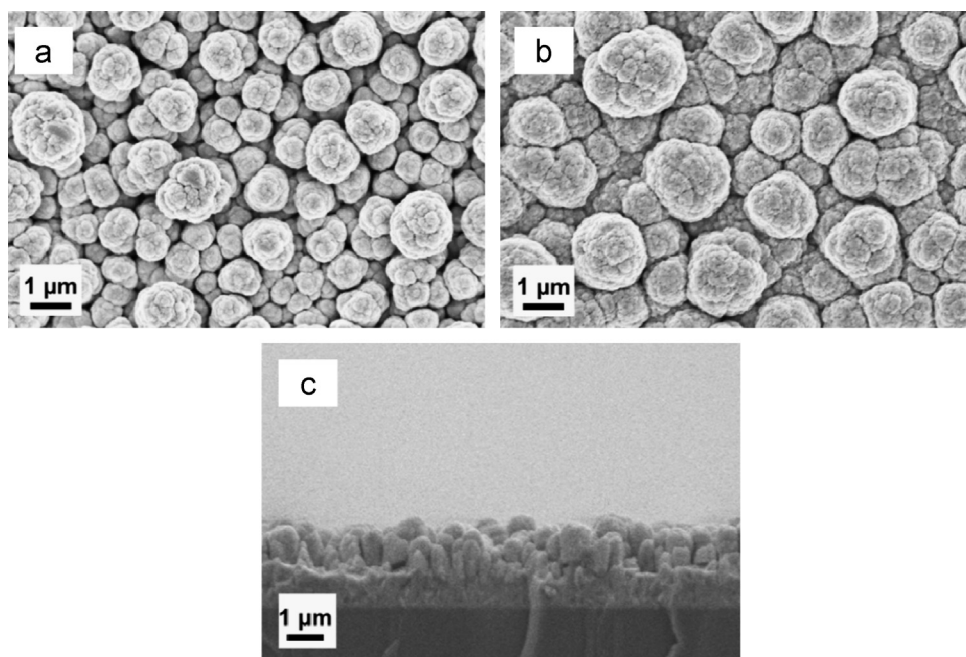


Fig. 2. SEM image of $\text{Bi}_2\text{Ti}_2\text{O}_7$ as deposited by AACVD (a), after annealing at $600\text{ }^\circ\text{C}$ for 12 h (b), and the cross-section of post-annealed $\text{Bi}_2\text{Ti}_2\text{O}_7$ (c).

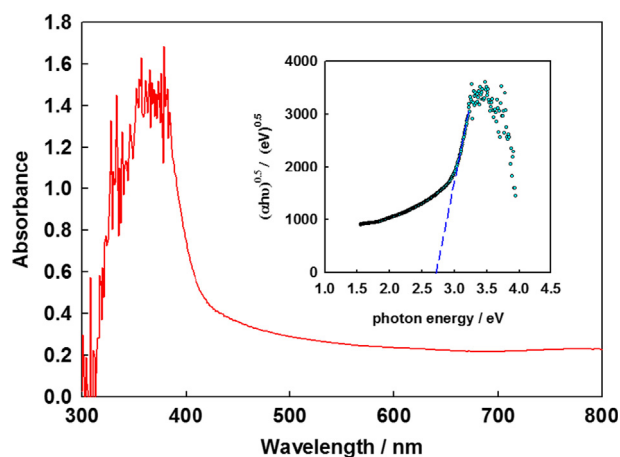


Fig. 3. UV-vis absorbance spectrum of $\text{Bi}_2\text{Ti}_2\text{O}_7$ prepared by AACVD after post-annealing. The inset shows a Tauc plot for $\text{Bi}_2\text{Ti}_2\text{O}_7$ which corresponds to a direct band gap of 2.74 eV.

estimated to be $-0.38\text{ V vs. Ag/AgCl}$. Taking into account the flatband potential and the band gap, the conduction and valence band energies are estimated to be 0.64 V and 3.38 V vs. NHE , respectively. This indicates that the valence band is sufficiently positive to give a large overpotential for water oxidation.

With our findings, we anticipate there to be an increase in interest in these materials, especially as it has been demonstrated recently that the band gap of $\text{Bi}_2\text{Ti}_2\text{O}_7$ can be further reduced by substitution of Fe and Mn into the structure, to as low as 2.2 eV [3,4]. Studies are currently under way to attempt to produce such substituted films by AACVD and investigate their PEC properties.

4. Conclusions

Phase pure $\text{Bi}_2\text{Ti}_2\text{O}_7$ thin films were prepared by AACVD for the first time. A post-deposition annealing step was necessary to improve the crystallinity of highly amorphous as-deposited thin films. The photoelectrochemical properties of $\text{Bi}_2\text{Ti}_2\text{O}_7$ thin films

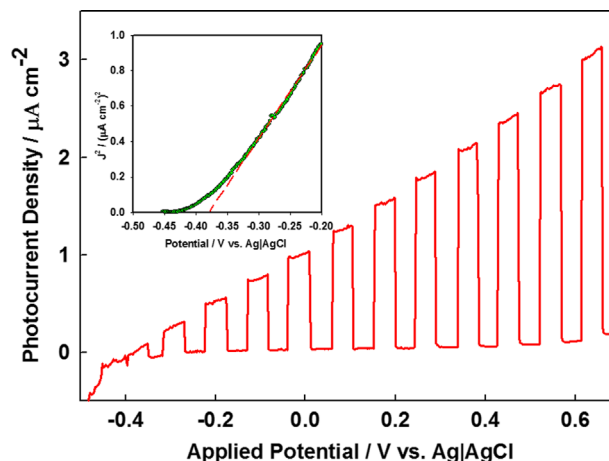


Fig. 4. Chopped current-voltage curve of $\text{Bi}_2\text{Ti}_2\text{O}_7$ produced by AACVD after 12 h post-annealing at $600\text{ }^\circ\text{C}$ under AM 1.5G illumination at 100 mW cm^{-2} intensity. The inset shows a plot of the square of the photocurrent as a function of applied potential to estimate the photocurrent onset.

were reported with a photocurrent density of $1.8\text{ } \mu\text{A cm}^{-2}$ at $0.23\text{ V vs. Ag/AgCl}$. The direct band gap of $\text{Bi}_2\text{Ti}_2\text{O}_7$ was calculated to be 2.74 eV . This shows that $\text{Bi}_2\text{Ti}_2\text{O}_7$ has the potential to be a more useful photoelectrochemical material than TiO_2 as it absorbs a greater proportion of the solar spectrum, has a direct band and exhibits less recombination.

Acknowledgements

AM acknowledges the support received from Engineering and Physical Sciences Research Council (Grant no. EP/G037116/1) through the Ph.D. studentship with the Doctoral Training Centre for Hydrogen, Fuel cells and their applications. The work was also supported by Loughborough University. The authors acknowledge the assistance given by the members of Energy Research Laboratory in the Department of Chemistry, Loughborough University.

References

- [1] Murugesan S, Huda MN, Yan Y, Al-Jassim MM, Subramanian V (Ravi). Band-engineered bismuth titanate pyrochlores for visible light photocatalysis. *J Phys Chem C* 2010;114:10598–605.
- [2] Kidchob T, Malfatti L, Marongiu D, Enzo S, Innocenzi P. Sol-gel processing of $\text{Bi}_2\text{Ti}_2\text{O}_7$ and $\text{Bi}_2\text{Ti}_4\text{O}_{11}$ films with photocatalytic activity. *J Am Ceram Soc* 2010;93:2897–902.
- [3] Gupta S, De Leon L, Subramanian VR. Mn-modified $\text{Bi}_2\text{Ti}_2\text{O}_7$ photocatalysts: bandgap engineered multifunctional photocatalysts for hydrogen generation. *Phys Chem Chem Phys* 2014;16:12719–27.
- [4] Allured B, De la Cruz S, Darling T, Huda MN, Subramanian V (Ravi). Enhancing the visible light absorbance of $\text{Bi}_2\text{Ti}_2\text{O}_7$ through Fe-substitution and its effects on photocatalytic hydrogen evolution. *Appl Catal B Environ* 2014;144:261–8.
- [5] Walsh A, Yan Y, Huda MN, Al-Jassim MM, Wei S. Band edge electronic structure of BiVO_4 : elucidating the role of the Bi s and V d orbitals. *Chem Mater* 2009;21:547–51.
- [6] Hinojosa B, Nino J, Asthagiri A. First-principles study of cubic Bi pyrochlores. *Phys Rev B* 2008;77:104123.
- [7] Yao WF, Wang H, Xu XH, Zhou JT, Yang XN, Zhang Y, et al. Photocatalytic property of bismuth titanate $\text{Bi}_2\text{Ti}_2\text{O}_7$. *Appl Catal A Gen* 2004;259:29–33.
- [8] Sato J, Kobayashi H, Ikarashi K, Saito N, Nishiyama H, Inoue Y. Photocatalytic activity for water decomposition of RuO_2 -dispersed Zn_2GeO_4 with d 10 configuration. *J Phys Chem B* 2004;108:4369–75.
- [9] Gupta S, Subramanian VR. Encapsulating $\text{Bi}_2\text{Ti}_2\text{O}_7$ (BTO) with reduced graphene oxide (RGO): an effective strategy to enhance photocatalytic and photoelectrocatalytic activity of BTO. *ACS Appl Mater Interfaces* 2014;7:10.1021/am503396r, in press.
- [10] Hector AL, Wiggan SB. Synthesis and structural study of stoichiometric $\text{Bi}_2\text{Ti}_2\text{O}_7$ pyrochlore. *J Solid State Chem* 2004;177:139–45.
- [11] Hou Y, Wang M, Xu X-H, Wang D, Wang H, Shang S-X. Dielectric and ferroelectric properties of nanocrystalline $\text{Bi}_2\text{Ti}_2\text{O}_7$ prepared by a metallorganic decomposition method. *J Am Ceram Soc* 2004;85:3087–9.
- [12] Cagnon J, Boesch DS, Finstrom NH, Nergiz SZ, Keane SP, Stemmer S. Microstructure and dielectric properties of pyrochlore $\text{Bi}_2\text{Ti}_2\text{O}_7$ thin films. *J Appl Phys* 2007;102:044102.
- [13] Tahir AA, Ehsan MA, Mazhar M, Wijayantha KGU, Zeller M, Hunter AD. Photoelectrochemical and photoresponsive properties of Bi_2S_3 nanotube and nanoparticle thin films. *Chem Mater* 2010;22:5084–92.
- [14] Tahir AA, Wijayantha KGU. Photoelectrochemical water splitting at nanostructured ZnFe_2O_4 electrodes. *J Photochem Photobiol A Chem* 2010;216:119–25.
- [15] Tahir AA, Wijayantha KGU, Saremi-Yarahmadi S, Mazhar M, McKee V. Nanostructured $\alpha\text{-Fe}_2\text{O}_3$ thin films for photoelectrochemical hydrogen generation. *Chem Mater* 2009;21:3763–72.
- [16] Dharmadasa R, Tahir AA, Wijayantha KGU. Single step growth and characterization of zinc oxide, tin oxide, and composite ($\text{Zn}_x\text{Sn}_{1-x}\text{O}_y$) nanoplate and nanocolumn electrodes. *J Am Ceram Soc* 2011;94:3540–6.
- [17] Tahir AA, Ehsan MA, Mazhar M, Wijayantha KGU, Zeller M, Hunter AD. Photoelectrochemical and photoresponsive properties of Bi_2S_3 nanotube and nanoparticle thin films. *Chem Mater* 2010;22:5084–92.
- [18] Tahir AA, Peiris T AN, Wijayantha KGU. Enhancement of photoelectrochemical performance of AACVD-produced TiO_2 electrodes by microwave irradiation while preserving the nanostructure. *Chem Vap Depos* 2012;18:107–11.
- [19] Peter LM, Wijayantha KGU, Tahir AA. Kinetics of light-driven oxygen evolution at $\alpha\text{-Fe}_2\text{O}_3$ electrodes. *Faraday Discuss* 2012;155:309.
- [20] Cummings CY, Marken F, Peter LM, Tahir AA, Wijayantha KGU. Kinetics and mechanism of light-driven oxygen evolution at thin film $\alpha\text{-Fe}_2\text{O}_3$ electrodes. *Chem Commun* 2012;48:2027–9.